Desalination and Water Treatment
www.deswater.com

doi: 10.1080/19443994.2016.1177736

57 (2016) 27672–27685
December

Taylor & Francis
Taylor & Francis Group

Nano-Fe_3O_4 and corn cover composite for removal of Alizarin Red S from aqueous solution: characterization and optimization investigations

J. Zolgharnein[a,*], Z. Choghaei[a], M. Bagtash[a], Sh. Feshki[a], M. Rastgordani[a], P. Zolgharnein[b]

[a]*Faculty of Science, Department of Chemistry, Arak University, Arak, Iran, emails: J-zolgharnein@araku.ac.ir, J.zolgharnein@gmail.com (J. Zolgharnein), Zch.Chemist@yahoo.com (Z. Choghaei), bagtash@yahoo.com (M. Bagtash), shahab.feshki@yahoo.com (Sh. Feshki), m.rastgordani@yahoo.com (M. Rastgordani)*
[b]*Material Science and Engineering Department, The University of Sheffield, Sheffield, UK, email: Pzolgharnein2@scheffild.ac.ir*

Received 26 November 2015; Accepted 7 April 2016

ABSTRACT

In this study, Fe_3O_4 nanoparticles impregnated onto corn cover were investigated as new composite sorbent for removing Alizarin Red S from aqueous solutions in a batch system. The main effective variables were examined on removal efficiency such as pH, sorbent dosage (m), and initial concentration of dye (C_d). Response surface methodology involving a Box–Behnken design for modeling the effective factors and their interactions was employed to optimize the removal percent ($R\%$) of Alizarin Red S dye. The best conditions for the suggested model was found to be the maximum removal percent of dye in pH 2, C_d = 10 mg/L and m = 0.2 g. The kinetics, isotherm modeling, and thermodynamic studies of adsorption Alizarin Red S were conducted. A second-order kinetic model is favorable for the dynamic behavior of the adsorption process. Thermodynamic studies indicate that the adsorption system was spontaneous and exothermic. Moreover, the structure and morphology of nanocomposite sorbent were examined by means of X-ray diffraction, EDX analysis, and scanning electron microscopy. Beside, FT-IR analyses were performed to characterize the functional groups which were involved in the adsorption process.

Keywords: Adsorption; Impregnated corn cover; Nano-Fe_3O_4; Box–Behnken design

1. Introduction

Dyes are among the most serious water pollutants, due to their wide use in many industries, causing health damage and environmental concerns [1–4]. Most organic dyes are harmful to human beings and toxic to plants and micro-organisms. Even if they are nontoxic, residual dyes in wastewater absorb sunlight, leading to a decrease in the efficiency of photosynthesis in aquatic plants [5]. Alizarin Red (AR) is among anionic dyes, which have been shown to have harmful effects on human beings [5–8]. This dye has been known to cause an allergic reaction and to be metabolized to Benzedrine. Its decomposition results in carcinogenic products [8]. However, the complex aromatic molecular structures of dyes make them more stable under light and they are categorized as non-biodegradable materials [1–3]. These dyes' hazardous effluent needs to be treated before being discharged into the environment [1–6]. Many physicochemical processes,

*Corresponding author.

such as chemical oxidation, adsorption, coagulation/flocculation, biological treatment, membrane separation, and ion exchange, are available for the removal of dyes from industrial effluents [9–19]. Among these methods, adsorption has been observed to be one of the most effective physical processes for the treatment of the wastewaters since it can produce high quality water and also be a process that is economically feasible [20,21]. Therefore, there has been a growing interest in finding low-cost alternative adsorbents with high adsorptive capacities and low production costs recently [1–3,20–22].

Since nanomaterials exhibit unique properties, as compared to conventional materials (zeolite, goethite, haematite, quartz sand, and activated carbon), research on nanomaterials has gradually become increasingly important and popular [23,24]. To date, nano-sized metal oxides, including nano-sized Fe_2O_3, Fe_3O_4, TiO_2, SiO_2, Al_2O_3, MgO, and CeO_2, have delivered some promising applications as adsorbents in water treatment [4–7,23–25]. This is due to their large surface areas and high activity levels, caused by the size quantization effect [23,24]. Among nano-sized metal oxides Fe_3O_4 nanoparticles beside their efficient, economic, scalable, and nontoxic synthesis adsorbent capacity, also have unique circumstances, due to facile separation from the solution rather than others sorbents [6,25]. Beside the nanoparticles sorbents properties, biosorbents have proved to be a low-cost sorbent with some advantages, as shown in the literature [1–4,23–28]. Recently, immobilization of nanoparticles with some proper biosorbents, such as agricultural residual, has significantly enhanced the efficiency of the adsorption process [26,27,29,30]. This result is due to a blend of advantages of both biosorbents and nanoparticles, and makes a new sorbent which increases its potential for pollutant removal [26,27,29,30].

Therefore, we have been motivated to investigate the immobilization of Fe_3O_4 nanoparticle on corn cover as a new adsorbent for the significant removal of Alizarin Red S from the aqueous solution. Since the capability of both mineral oxides and biosorbents to the adsorptive removal of pollutants is strongly influenced by some parameters, such as pH, time, temperature, the initial concentration of pollutants, and sorbent mass [6–8,28,31–35], it is crucial to design a proper process for maximizing the removal efficiency of pollutants by this new adsorbent [7,8,28,31–37]. In regard to the advantages of multivariate optimization which have recently been revealed, especially experimental design rather than the conventional "one-at-a-time" method has attracted interests in relation to optimization of adsorption process [35–37]. It is well known that experimental design provides more information with fewer experiments, running a response surface methodology (RSM) which leads to an empirical mathematical model in relation to the removal percent ($R\%$) of sorbate with effective variables and their interactions [7,8,28,31–37].

However, in this study the potential of both the Fe_3O_4 nanoparticle and corn cover and the immobilizing of them as an efficient adsorbent along with finding optimum conditions by a Box–Behnken design (BBD) approach is investigated. The characterizations of sorbents, isotherm modeling, kinetic studies and the thermodynamic behavior of adsorption of Alizarin Red S on this new adsorbent is also considered in details.

2. Materials and methods

2.1. Preparation biosorbent

Corn covers were gathered from a grove in a suburb at Markazi Province, Iran. The collected materials were then washed with distilled water several times to remove all the dirt particles. The dried biomass was pulverized well in a mixer and sieved (100–150 μm) and stored in a bottle.

2.2. Reagents and equipment

All chemicals used during the process were of analytical grade. Alizarin Red S (Fluka), HCl (Merck, Darmstadt, Germany), Fe_3O_4 nanoparticle (TENCAN). Double-distilled water was used for each run. A pH meter (Metrohm, model 744), UV/VIS spectrophotometer (Analytikjena double beam SPECORD250), FTIR (Unicam-Galaxy series FT-IR 5000), and X-ray diffraction (XRD; Philips) were used. The scanning electron microscopy (SEM) measurements were carried out using TESCAN (VEGA3).

2.3. Preparation of nano-Fe_3O_4/corn cover composite

A proper amount of Fe_3O_4 nanoparticle and corn cover with different ratios from 1:20, 1:10, 1:5, 1:2, and 1:1 (nano-Fe_3O_4: corn cover) were grounded well and transferred to an Erlenmeyer containing double-distilled water and mixed well in a shaker at 300 rpm for 2 d, then in a 70°C oven for five hours to dry.

2.4. Adsorption studies

A stock solution of dye was prepared by dissolving 1.0 g of Alizarin Red S in 1,000 mL of

double distilled water. Standard solutions of dye were made by dilution of the stock solution. The pH of the solution was adjusted by HNO_3 and NaOH 0.1 M. A known amount of adsorbent was added to the sample and allowed sufficient time for reaching adsorption equilibrium. Then the mixture were filtered and the remaining dye concentration determined in the filtrate using (Spectro UV–vis Double Beam UVD) at λ_{max} = 423 nm. The dye removal and equilibrium adsorption capacity (q) was determined according to Eqs. (1) and (2), respectively:

$$R\% = \frac{C_0 - C_e}{C_0} \times 100 \quad (1)$$

$$q_e = \frac{(C_0 - C_e)V}{M} \quad (2)$$

where C_0 (mg/L) is the initial concentration and C_e (mg/L) is the concentration of the dye at equilibrium, q_e is the amount of dye adsorbed onto the sorbent at equilibrium (mg/g), V is the volume of the solution (L), and M is the mass of sorbent (g) [7].

2.5. Adsorbent analysis

The Fourier transform infrared (FTIR) spectra of adsorbent in the range of 400–4,000 cm^{-1} were taken using a Unicam-Galaxy series FT-IR 5000, to identify functional groups of adsorbent involved. In addition, an X-ray diffraction (XRD) pattern of the sorbent was recorded using a Philips X-ray diffractometer (model PW 3040/60 X'pert pro). The XRD measurements were made over a range of 30–50˚, using a Phillips powder diffractometer model PW3040 with Cu K_α radiation at a scan speed of 1˚/min. The SEM images were taken at high voltages (20 kV).

2.6. Optimization using RSM

The RSM is an efficient method for the optimization of the adsorption process for a multi-variable approach with a minimum number of experiments using a set of designed experiments [37,38]. The BBD is among RSM, which is a spherical, rotatable, or nearly rotatable second-order design. It is based on a three-level incomplete factorial design, which consists of the center point and middle points of the edges from a cube. The number of experimental points (N) is defined by the expression $N = 2k(k - 1) + C_0$, where k is the number of variables and C_0 is the number of center points [31,37–40]. The most significant advantage of the BBD matrix is to avoid experiments performed under extreme conditions, for which unsatisfactory results might occur [31,39,40]. In the present study, by employing the BBD, the effect of the three independent variables on the removal percent ($R\%$) were investigated and the relation to experimental design was obtained.

3. Results and discussion

3.1. Effect of different adsorbent ratio (nano-Fe_3O_4/corn cover)

The effect of three different adsorbents, i.e. corn cover, nano-Fe_3O_4, and nano-Fe_3O_4/corn cover composite at the percentage removal of Alizarin Red S dye were investigated. The settings of the parameters were based on the following: an initial concentration 50 mg/L; an adsorbent dosage of 0.1 g, temperature 298 K for 70 min; and a shaking speed of 300 rpm. The percentage removal ($R\%$) obtained for the nano-Fe_3O_4/corn cover composite (1:10), nano-Fe_3O_4 and Corn cover were 80.1, 65.5, and 2.8%, respectively (Fig. 1). The percentage removal of Alizarin Red S using different adsorbent ratios (nano-Fe_3O_4/corn cover), such as 1:20, 1:10, 1:5, 1:2, and 1:1 were considered. The percentage removal increases with a decreasing nano-Fe_3O_4 ratio, but the removal remained almost constant after 1:10 ratio. This ratio is suitable for use in the removal of dye since the surface area of corn cover is completely occupied by nano-Fe_3O_4 [29].

3.2. FT-IR analysis

The FT-IR spectra of Alizarin red S, nano-Fe_3O_4/corn cover composite and loaded sorbent with dye are shown in Fig. 2(a)–(c) and the corresponding infrared

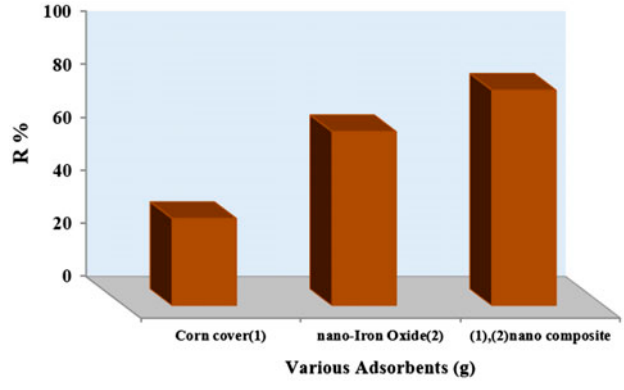

Fig. 1. The percentage of dye removal by: (1) after corn cover, (2) nano-Fe_3O_4 and (3) nano-Fe_3O_4/corn cover composite.

absorption frequency of functional groups is reflected in Table 1. In all spectra, the bonded OH groups are observed in the range of 3,387–3,447 cm^{-1}. The band observed at about 2,922 cm^{-1} could be assigned to the aliphatic C–H group of sorbent. The peak observed at 1,433 and 1,518 cm^{-1} corresponds to the aromatic C=C group and bending of CH_3 stretching is observed at 1,443 cm^{-1}. In the case of Fe_3O_4 (Fig. 2(b)), the broad absorption band at 3,387 cm^{-1} indicates the presence of surface hydroxyl groups (O–H stretching) and the bands at lower wave numbers 700 (≤700 cm^{-1}) are related to vibrations of the Fe–O bonds in Fe_3O_4 [29]. Also the two small peaks at 351 and 584 cm^{-1} are related to the Fe–O group (Fig. 2(b)) [29,41–43]. The comparison of spectra in Fig. 2 shows that some peaks shifted or disappeared and new peaks were produced. For example, the stretching vibration of OH group was shifted from 3,387 to 3,412 cm^{-1} in the dye-loaded composite. These results reveal that chemical interactions between the dye and the hydroxyl groups sorbent occurred on the surface. Finally, the comparisons of the FT-IR spectrum of unloaded adsorbent (Fig. 2(b)) and loaded adsorbent (Fig. 2(c)) show the changing and shifting of many bands(for Fe–O: from 582 to 569 cm^{-1}, Table 1), which confirm that most functional groups present in the nano-Fe_3O_4/corn cover composite are involved with Alizarin Red S during the adsorption process [29,41–43].

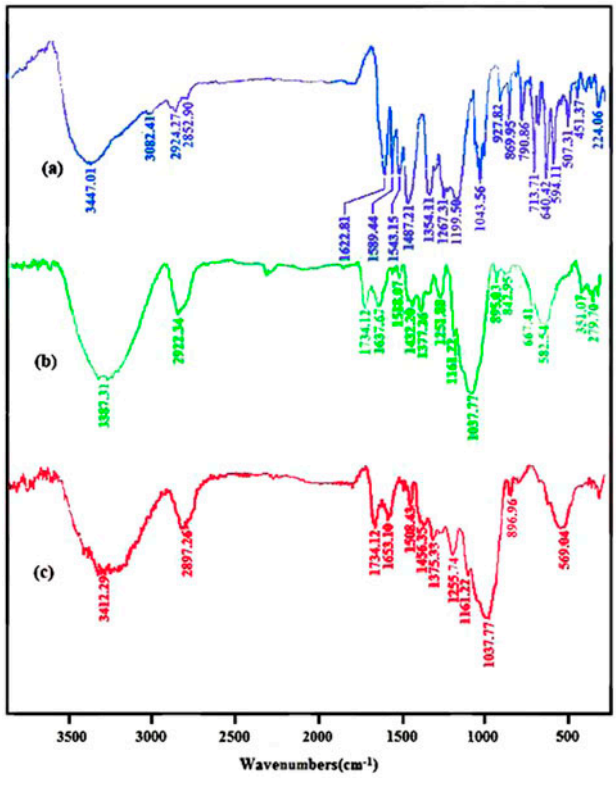

Fig. 2. FT-IR spectra of (a) Alizarin Red S, (b) unloaded nano-Fe_3O_4/corn cover composite, and (c) loaded nano-Fe_3O_4/corn cover composite.

3.3. XRD, SEM, and EDX analysis

The XRD patterns for samples corn cover (a), nano-Fe_3O_4 (b), and nano-Fe_3O_4/corn cover composite (c) are shown in Fig. 3. The diffraction peaks of nano-Fe_3O_4 at angles of 2θ = 21.35, 35.17, 41.48, 43.43, 50.55, 62.98, 67.30, and 74.24 can be assigned. The diffraction peaks of Fe_3O_4 in the nano-Fe_3O_4/corn cover composite confirmed that the Fe_3O_4 nanoparticles impregnated onto the biosorbent (corn cover) and nanocomposite was formed [29,42]. SEM images depict the surface of particles for the samples of the pristine corn cover (a), nano-Fe_3O_4/corn cover (b), and nano-Fe_3O_4/corn cover-loaded dye (shown in Fig. 4). The corn cover has insoluble cell walls with fibrous content and is largely made up of cellulose. Fig. 4(b) shows the corn cover is completely covered with nano-Fe_3O_4, and all the nano-Fe_3O_4 particles are aggregated to form a spherical and cage-like structure. Fig. 4(c) also shown the loading of dye on both nano-Fe_3O_4 and corn cover surfaces. EDX spectra are also included for both pristine corn cover (a) and nano-Fe_3O_4/corn cover composite (b) are presented in Fig. 4, where peaks associated with Fe, C, and O can be distinguished [29,43].

3.4. Optimization of adsorptive removal process by statistical experimental design

The optimal conditions for the adsorption removal of Alizarin Red S by nano-Fe_3O_4/corn cover composite were determined by means of BBD [31,37–40]. Multivariate optimization studies were performed by considering the effect of three variables, including adsorbent dosage (m), initial concentration of dye (C_d), and pH of solutions. In BBD for three-variables and three replicates in center point according to $N = 2k(k - 1) + c_p$ was run with 15 experimental points. All factor levels had to be adjusted only at three levels (−1, 0, +1), with equally coded units from RSM studies given in Table 2. The chosen independent variables used in this study were coded according to Eq. (3) [38]:

$$X_i = (A_i - A_0)/\Delta A_i \quad (3)$$

where X_i is a coded value of the variable, A_i is the real value of variable, A_0 is the real value of A_i at the center point and ΔA_i is the step change of variable

Table 1
The FT-IR peaks for nano-Fe_3O_4/corn cover composite

IR peaks	Assignment	υ (cm^{-1})		
		[a]Sorbent	[b]Alizarin Red	[c]Loaded sorbent
1	O–H	3,387	3,447	3,412
2	Aromatic C–H	–	3,082	–
3	Aliphatic C–H	2,922	2,924	2,897
4	C=O	1,637	1,589	1,653
5	Aromatic C=C	1,433	1,487	1,456
		1,518	1,543	1,508
6	CH_3 stretching	1,377	1,354	1,375
7	$-SO_3$	1,251	1,267	1,255
8	C–O	1,037	1,043	1,037
9	Fe–O	582	–	569
		351		365

[a]Fig. 2(b)
[b]Fig. 2(a).
[c]Fig. 2(c).

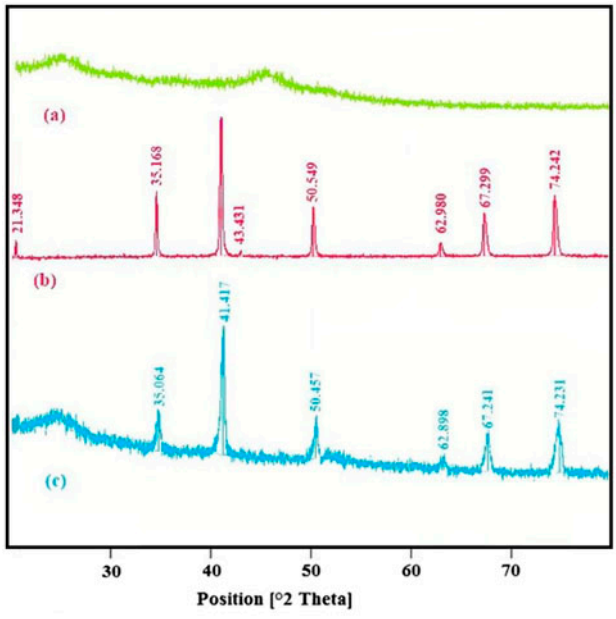

Fig. 3. XRD spectra of (a) corn cover, (b) nano-Fe_3O_4, and (c) nano-Fe_3O_4/corn cover composite.

[39,40]. Minitab statistical software version 15 was utilized for handling data. Main effects, interactions between factors, coefficients, standard deviation of coefficients, and other statistical indices of the fitted model and statistical plots were the output data of this software [37–40]. Table 3 shows the results of BBD experiments for studying the effect of three independent variables. The effects, regression coefficients, standard errors, and T and p-values for the removal of dye are exhibited in Table 4 (at a 95% confidence level). The effect of all the linear terms, such as dye concentration (C_d), pH, and adsorbent amount (m) on the responses of $\%R$ were found to be highly significant because p-values were less than 0.05 (other parameters, where p-values were more than 0.05, were eliminated) [36–39].

3.4.1. Modeling the adsorptive removal process

One of the huge application advantages of RSM is estimation of mathematical relationships between the response function (Y) and the independent variables (X) by a quadratic polynomial equation, as follows [40]:

$$Y = b_0 + \sum_{i=1}^{k} b_i x_i + \sum_{i=1}^{k} b_{ii} x_i^2 + \sum_{i=1}^{k} \sum_{j=1}^{k} b_{ij} x_i x_j + \varepsilon \quad (4)$$

where Y is the predicted response (removal percent), b_0 the constant coefficient, b_i the linear coefficients, b_{ii} the quadratic coefficients, b_{ij} the interaction coefficients and x_i, x_j are the coded values of the variables [40]. The coefficients of the response function for different dependent variables were determined. The effect of all the linear terms, such as Alizarin Red S concentration, pH, and sorbent amount (m), in responses of $\%R$ were found to be highly significant because p-values were less than 0.05 (Table 4) [36,37]. Then a second-order polynomial equation in coded form was established to explain the empirical relationship between the Alizarin Red S removal percent ($R\%$) and the three variables obtained by the application of RSM, as given below:

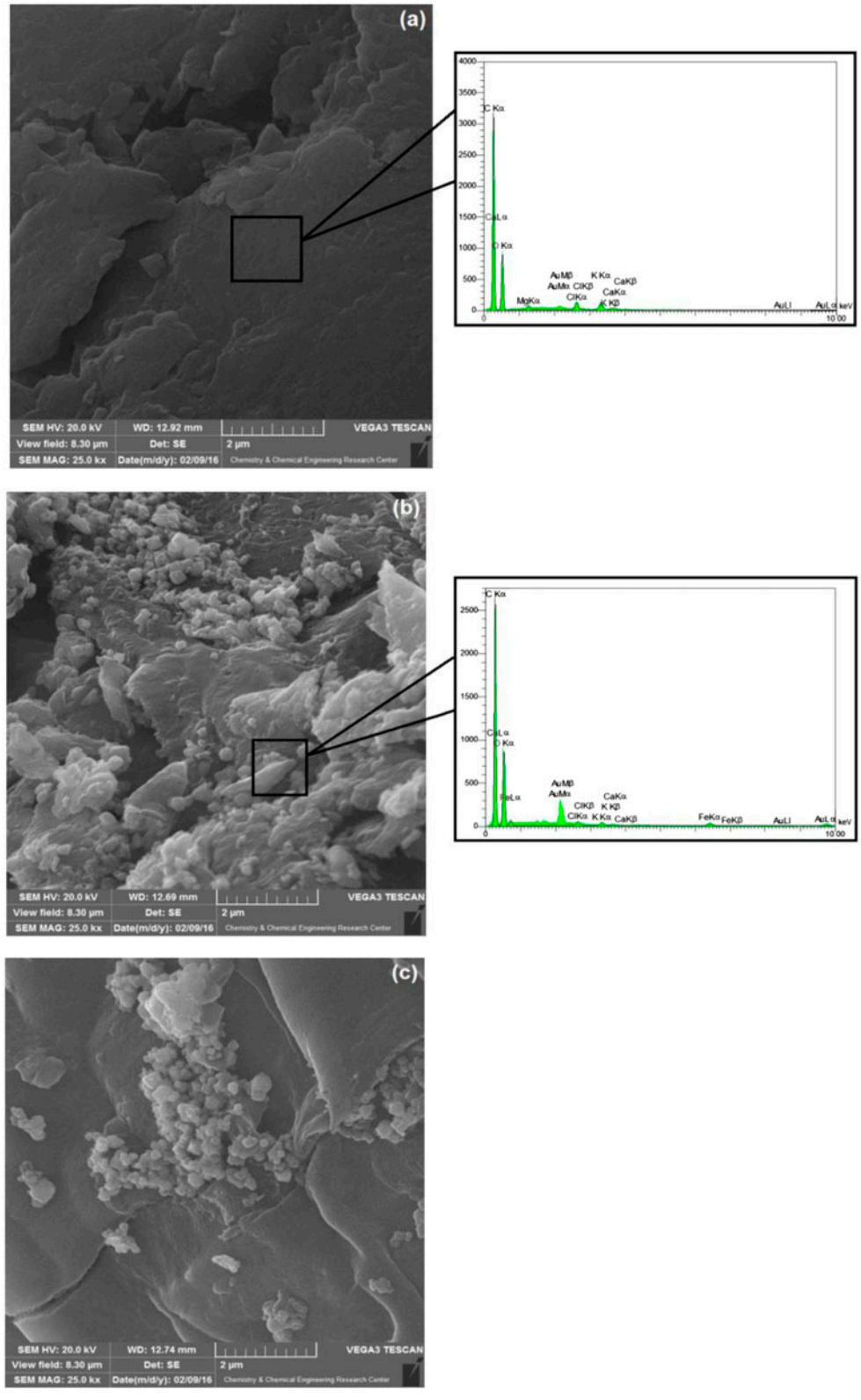

Fig. 4. SEM micrograph of (a) corn cover, (b) nano-Fe_3O_4/corn cover composite, and (c) nano-Fe_3O_4/corn cover composite-loaded dye, along with EDX of (a) corn cover, (b) nano-Fe_3O_4/corn cover composite.

Table 2
Factors and their levels used in the BBD design

Independent variable unite		Coded levels		
		−1	0	+1
pH	–	2	4	6
Initial concentration of dye (C_d)	C_d: mg/L	10	205	400
Dosage of sorbent (m)	g	0.025	0.1375	0.25

Table 3
BBD and results obtained for removal of Alizarin Red S

Run order	pH	C_d	m	R%	q
1	2(−1)	205(0)	0.025(−1)	46.1	37.8
2	2(−1)	205(0)	0.25(+1)	82.6	6.8
3	2(−1)	10(−1)	0.1375(0)	93.6	0.7
4	6(+1)	10(−1)	0.1375(0)	68.5	0.5
5	6(+1)	205(0)	0.025(−1)	21.0	17.2
6	4(0)	10(−1)	0.025(−1)	50.4	2.0
7	6(+1)	205(0)	0.25(+1)	75.4	6.2
8	2(−1)	400(+1)	0.1375(0)	59.6	17.3
9	4(0)	400(+1)	0.25(+1)	39.6	10.2
10	6(+1)	400(+1)	0.1375(0)	29.5	11.5
11	4(0)	10(−1)	0.25(+1)	91.4	0.4
12	4(0)	205(0)	0.1375(0)	46.7	6.9
13	4(0)	205(0)	0.1375(0)	46.6	6.8
14	4(0)	205(0)	0.1375(0)	42.9	6.4
15	4(0)	400(+1)	0.025(−1)	10.26	16.41

Notes: C_d: Initial concentration of dye; m: dosage of sorbent.

Table 4
The effects, regression coefficients, standard errors, and T and p-values for the removal of dye

Term	Coef.	SE Coef.	T	p
Constant	45.252	1.158	39.086	0.000
pH	−9.644	0.8521	−11.318	0.000
C_d	−16.330	0.8521	−19.165	0.000
m	23.190	0.8521	27.215	0.000
pH × pH	11.129	1.250	8.899	0.000
$C_d \times C_d$	8.821	1.250	7.054	0.000
pH × m	4.487	1.205	3.723	0.000
$C_d \times m$	3.110	1.205	2.581	0.007

$$\%R = 45.25 - 9.66\,\mathrm{pH} - 16.33\,C_d + 23.19\,m + 11.13\,\mathrm{pH}^2 + 8.82\,C_d^2 + 4.49\,\mathrm{pH} \times m + 3.11\,C_d \times m \quad (5)$$

Recognition of the significant main and interaction effects of factors affecting the removal efficiency was followed by the application of an analysis of variance (ANOVA). Since all runs were carried out in duplicate, an estimation of error or residue was used to define the statistically significant factors for the removal percent of Alizarin Red S, based on ANOVA. The sum of squares (SS) is used to estimate the F-ratios (F), which are defined as the ratio of the respective mean square effect (MS_{effect}) and the mean square error (MS_{error}) (see Table 5). The lack of fit term, 0.462, was insignificant ($p > 0.05$) and also the regression was meaningful ($p < 0.05$) for all responses (Table 5). Therefore, the second-order polynomial model was highly significant and fitted well to the experimental results. The coefficient of determination for R% response was computed as $R^2 = 0.9732$, which is a measure of the amount of variation around the mean, as explained by the model, and so only 0.51% of total variance was not explained by the model [36,37]. The correspondingly predicted R^2 (0.9732) for the removal percent of dye is close to 1.0, which indicates a high predictability of the model. The residual analysis also had to be evaluated for normal distribution and represented that they had no obvious pattern or unusual structure, which confirms the adequacy of the obtained model [36,37]. The response surface plots shown in Fig. 5(a)–(c) were prepared by the Minitab software and utilized to indicate the influence of the experimental factors on Alizarin Red S removal percent (R%) [8,28]. The best conditions for the suggested model was found to be the maximum removal percent of dye in pH 2, C_d = 10 mg/L and m = 0.2 g.

3.5. Adsorption isotherms modeling

The consideration of dye and adsorbent equilibrium behavior through finding proper isotherm modeling is a major concern in relation to the adsorption process. Finding the equilibrium relationship between the quantity of dye uptake per unit of adsorbent (q_e) and its equilibrium solution concentration (C_e) at a constant temperature is essential to the design and optimization of an adsorption process [44–46].

Table 5
ANOVA for the suggested model

Source	DF	Sum of square	Mean square	*F*-value	*p*-value
Regression	7	7,999.21	1,142.74	196.74	0.000
Residual error	7	40.66	5.81		
Lack of fit	5	31.74	6.35	1.42	**0.462**
Pure error	2	8.92	4.46		
Total	14	8,039.87			

Notes: DF: degree of freedom.

3.5.1. Langmuir isotherm

The basic assumption of the Langmuir theory is that the adsorption takes place at specific homogeneous sites within the adsorption, which is a monolayer too [7,8,31–33,44–46]. The linear form of the Langmuir isotherm is shown as follows:

$$\frac{C_{eq}}{q_{eq}} = \frac{1}{bq_{max}} + \frac{C_{eq}}{q_{max}} \quad (6)$$

where C_{eq} (mg/L) is the concentration of the dye solution at equilibrium, q_{eq} (mg/g) is equilibrium uptake capacity, and q_{max} is the maximum uptake capacity and b is the Langmuir constant. The q_{max} and b values from the slopes ($1/q_{max}$) and intercepts ($1/bq_{max}$) of the linear plot of C_e/q_e vs. C_e in Fig. 6 were calculated and are as: 10.52 mg/g, and 0.030 L/mg ($R^2 = 0.973$), respectively. The nonlinear regression analysis of the Langmuir equation leads to q_{max} and b values, thus: 11.35 mg/g and 0.029 L/mg ($R^2 = 0.995$, $\chi^2 = 0.239$) [47].

3.5.2. Freundlich isotherm

The Freundlich equilibrium isotherm equation is an empirical equation which applies to adsorption onto heterogeneous surfaces with the same energy distribution and reversible adsorption. This isotherm is expressed by Eq. (7) where C_{eq} (mg/L) and q_{eq} (mg/g) are the liquid phase concentration and solid phase concentration of the adsorbate at equilibrium, respectively [7,8,31–33,44–46]:

$$q_{eq} = K_F C_{eq}^{1/n} \quad (7)$$

A linear form of this equation is:

$$\ln q_{eq} = \frac{1}{n} \ln C_{eq} + \ln K_F \quad (8)$$

where K_F is the Freundlich constant (L/mg) and $1/n_F$ is the heterogeneity factor, which were determined by the intercept and slope of Fig. 7, and the results are $K_F = 0.852$ L/mg, and $1/n_F = 0.45$ ($R^2 = 0.980$); and nonlinear regression of Eq. (7) yields $K_F = 1.34$ L/mg, $1/n_F = 0.41$ ($R^2 = 0.982$, $\chi^2 = 0.287$) [31,32,48]. When $1/n$ lies between 0 and 1, it illustrates a favorable adsorption [44–47,49].

3.5.3. Dubinin–Radushkevich isotherm

The Dubinin–Radushkevich model is often applied to estimate the characteristic porosity and the apparent free energy of adsorption. Thus, methods of evaluating these parameters for the adsorbents the D–R isotherm have been investigated [44–49]. The linear form of the D–R equation is given as follows:

$$\ln q_{eq} = \ln q_{max} - \beta\varepsilon^2 \quad (9)$$

$$\varepsilon = RT \ln\left(1 + \frac{1}{C_{eq}}\right) \quad (10)$$

A plot of $\ln q_{eq}$ vs. ε^2 gives a straight line (Fig. 8). The constant B gives the mean free energy E of sorption per molecule of sorbate when it is transferred to the surface of the solid from the bulk solution, and can be computed using the following relationship:

$$E = \frac{1}{\sqrt{2\beta}} \quad (11)$$

From the magnitude of E, the types of adsorption, such as chemisorption or physical sorption can be determined. If E = 8–16 kJ/mol, then chemical ion-exchange dominates the reaction. If $E < 8$ kJ/mol, then physical adsorption takes place, while chemisorption processes have adsorption energy in the range of 20–40 kJ/mol [31,32,43,48,49]. The mean free energy of adsorption of Alizarin Red S onto nano-Fe_3O_4/corn cover composite (E) is found to be 12.91 kJ/mol and chemical ion exchange may be the dominate

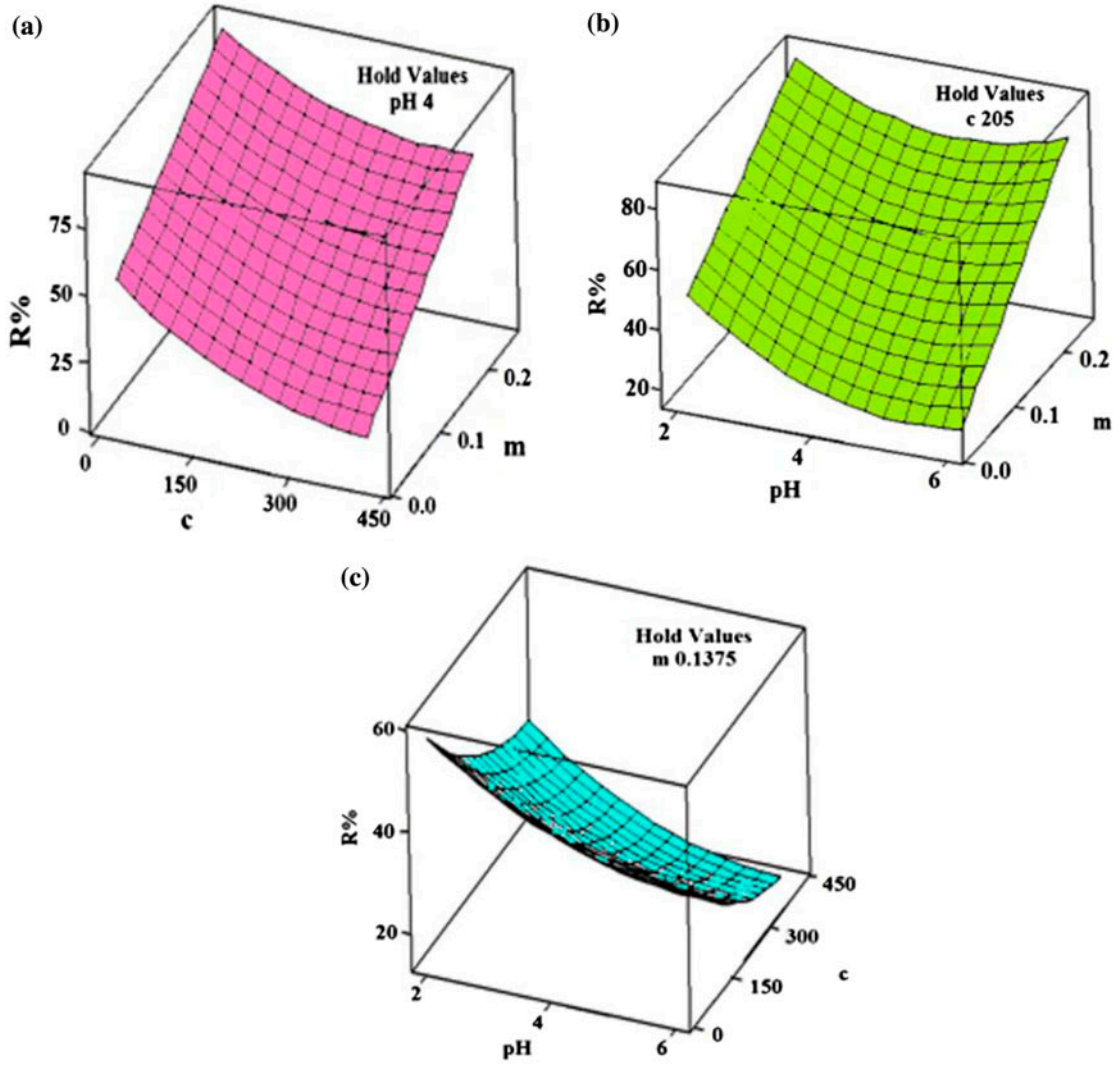

Fig. 5. Response surface plots of the quadratic model: (a) the effect of dye concentration (C_d) and adsorbent dosage (m) on the $R\%$, while the pH was kept constant at its optimum value, (b) The effect of the adsorbent dosage (m) and pH on the $R\%$ while dye concentration was kept constant at its optimum value, (c) The effect of dye concentration (C_d) and pH on $R\%$ while the adsorbent dosage (m) was kept constant at its optimum value.

interaction [31,32,44,48–50]. According to R^2 values (R^2 = 0.973, 0.980, 0.995), Langmuir, Freundlich, and Dubinin–Radushkevich isotherms successfully describe the equilibrium behavior of Alizarin Red S adsorption by nano-Fe_3O_4/corn cover composite adsorbent (results are listed in Table 6) [47].

3.6. Kinetic studies

The kinetic of the adsorption process of dye plays an important role in the predication of rate of decontamination of dye from an aqueous source. Moreover, it describes the dye uptake rate and controls the residence time of the adsorption process [31,32,44,45]. So, in order to examine the adsorption kinetics of Alizarin Red S on a nano-Fe_3O_4/corn cover composite, three models were used, including pseudo-first-order, pseudo-second-order, and intraparticle diffusion models [44–46].

3.6.1. Pseudo-first-order model

The linear form of the pseudo-first-order equation is given as follows:

$$\ln(q_e - q_t) = \ln q_e - k_1 t \quad (12)$$

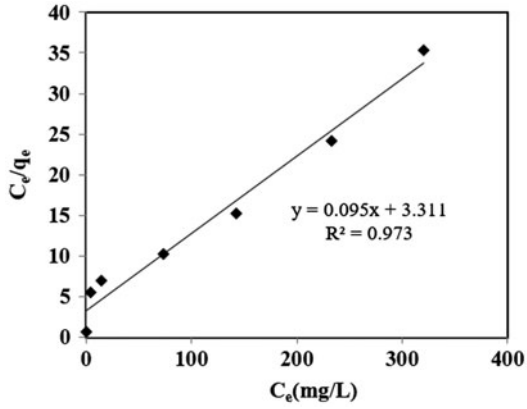

Fig. 6. The linear Langmuir adsorption isotherms for Alizarin Red S by nano-Fe_3O_4/corn cover composite.

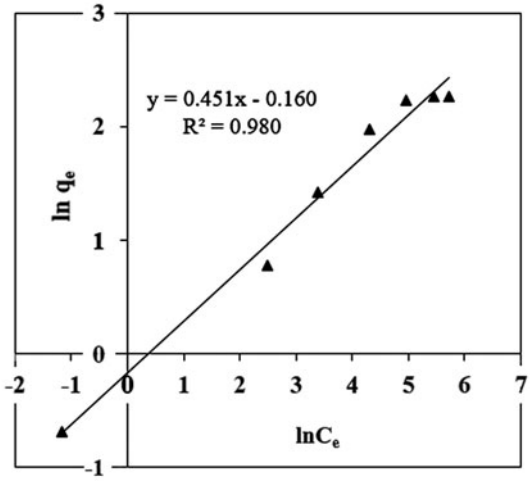

Fig. 7. The linear Freundlich adsorption isotherms for Alizarin Red S by nano-Fe_3O_4/corn cover composite (conditions: pH 2, m = 0.2 g).

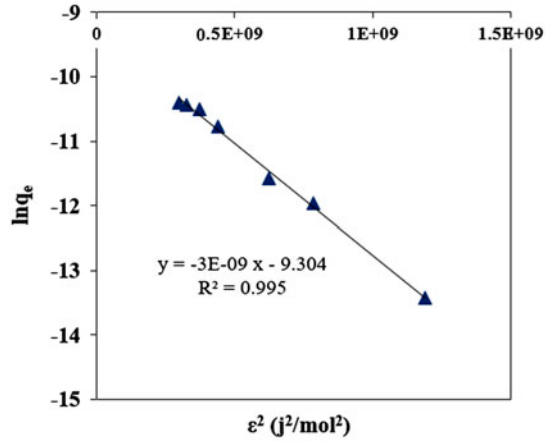

Fig. 8. The D–R adsorption isotherms for Alizarin Red S by nano-Fe_3O_4/corn cover composite (conditions: pH 2, m = 0.2 g).

Table 6
Parameters of Langmuir, Freundlich, and D–R isotherms for the adsorption of Alizarin Red S

Langmuir model				
	q_{max} (mg/g)	b (l/mg)	R^2	χ^2
Linear	10.52	0.030	0.973	–
Nonlinear	11.35	0.029	0.995	0.239
Freundlich model				
	K_f	n	R^2	χ^2
Linear	0.852	2.22	0.980	–
Nonlinear	1.34	2.42	0.982	0.287
D–R model				
q_{max} (mg/g)	β (mol^2/KJ^2)	E (kJ/mol)	R^2	χ^2
31.16	0.003	12.91	0.995	–

Notes: Conditions: pH 2, m = 0.2 g.

where q_t is the amount of dye adsorbed at time t (mg/g), q_e the capacity uptake at equilibrium (mg/g), k_1 the pseudo-first-order rate constant (1/min), and t the contact time (min). The values of the adsorption rate constant (k_1 = 0.038 1/min) for Alizarin Red S adsorption were determined from the plot of ln ($q_e - q_t$) vs. t and q_e can be determined from the intercept plot in Fig. 9; the result is q_{eq} = 10.39 mg/g, as shown in Table 6.

3.6.2. Pseudo-second-order model

The pseudo-second-order model is represented as:

$$\frac{t}{q_t} = \frac{1}{k_2 q_e^2} + \frac{t}{q_e} \quad (13)$$

where k_2 (g/(mg min)) is the rate equilibrium constant of pseudo-second-order reaction. The q_e (mg/g) is obtained from the slope of t/q_t vs. t (Fig.10). Since q_e (10.98 mg/g) is known from the slope, the k_2 (0.117 g/(mg min)) can be determined from the intercept plot. The data did not fit well to the first-order equation in the entire region of Alizarin Red S concentration used in this work (R^2 = 0.884), but it did fit very well with the pseudo-second-order model (R^2 = 0.998) and the calculated q_e values also agreed well with the experimental data. These results suggest that the overall rate of the Alizarin Red S adsorption process appears to be controlled by the chemical adsorption or chemisorption process [31,32,48,50,51] (results are given in Table 6).

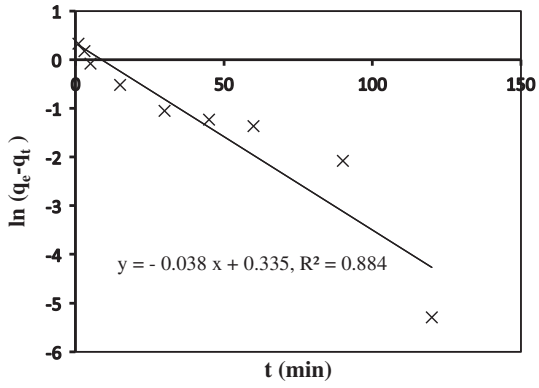

Fig. 9. Alizarin Red S adsorption by nano-Fe_3O_4/corn cover composite on the pseudo-first-order model (conditions: pH 3, m = 0.2 g, C_d: 200 mg/L).

3.6.3. Intraparticle diffusion model

The intraparticle diffusion model was introduced by Weber and Morris [52].

The equation utilized is as follows:

$$q_t = K_{id}t^{1/2} + C \quad (14)$$

where q_t (mg/g) is the amount adsorbed at time t (min), K_{id} (mg/(g min$^{0.5}$)) is the rate constant of intra-particle diffusion, and C is the value of intercept which gives an idea about the boundary layer thickness. If intraparticle diffusion is rate limited, then plots of dye uptake (q_t) vs. $t^{1/2}$ would result in a linear relationship. If the plot of q_t vs. $t^{1/2}$ is linear and passes through the origin, then intraparticle diffusion is the only rate-limiting step [48–51]. Theoretical consideration of kinetic mechanism of adsorption of Alizarin Red S onto nano-Fe_3O_4/corn cover might exhibit three stages in practice. Due to mass transfer of the dye onto the surface of the sorbent, the first step is usually fast and impossible to monitor precisely. Second, intraparticle diffusion into pores and the cell wall of the sorbent may occur. The third step involves reaching equilibrium after about 50 min corresponding to the involvement of Alizarin Red S in the interior pore structure of sorbent [31,48–54].

Fig. 11 shows that the linear part of plots does not pass through the origin (C = 0.999, 1.933, 2.681). This represents some degree of boundary layer control and then intraparticle diffusion is not only the rate which determines the step in the kinetic activity of the adsorption process of Alizarin Red S (Fig. 11) [31,32,48–54]. The increase in K_{id} values (0.287, 0.372, 0.602 mg/(g min$^{0.5}$)) with increasing initial dye concentrations (100, 200, 300 mg/L) can be illustrated by growing the effect of the driving force, which resulted in reducing the diffusion of dyes in the boundary layer and enhancing the diffusion in the solid sorbent. All kinetic results are given in Table 7.

3.7. Thermodynamic parameters

Thermodynamic behavior of the adsorption of Alizarin Red S onto a nano-Fe_3O_4/corn cover composite was evaluated by finding thermodynamic parameters, including the changes in free energy and entropy. These factors must be considered in order to determine what processes will occur spontaneously

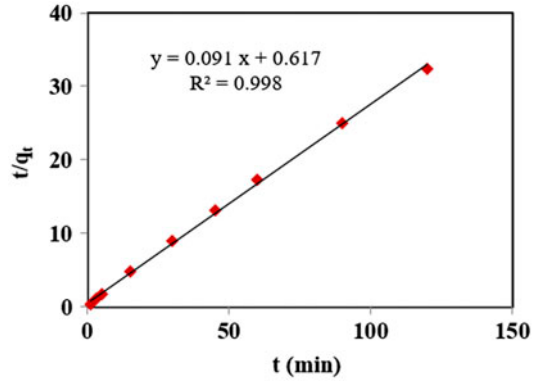

Fig. 10. Alizarin Red S adsorption by nano-Fe_3O_4/corn cover composite on the pseudo-second-order model. (Conditions: pH 3, m = 0.2 g, C_d: 200 mg/L).

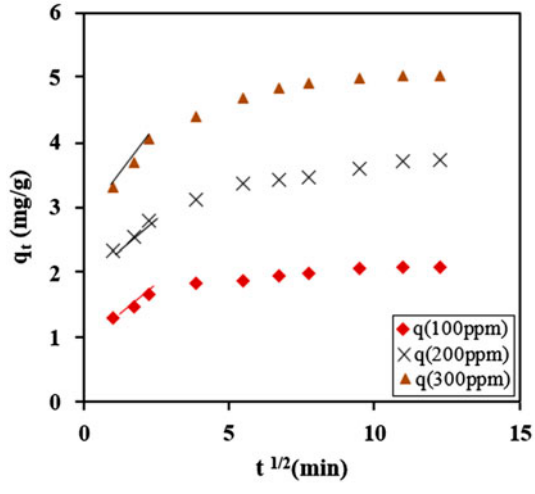

Fig. 11. Intra-particle diffusion plot of Alizarin Red S adsorption by nano-Fe_3O_4/corn cover composite (conditions: pH 3, m = 0.2 g).

Table 7
Kinetic parameters for removal of Alizarin Red S

		Pseudo-first-order equation		
C_0 (mg/L)	q_{exp}	q_{eq} (mg/g)	K_1 (min^{-1})	R^2
100	10.75	10.39	0.038	0.884
		Pseudo-second-order equation		
		q_{eq} (mg/g)	K_2 (g/mg min)	R^2
100	10.75	10.98	0.117	0.998
		Intraparticle-diffusion equation		
		C	K_{ind} (mg/g $min^{0.5}$)	R^2
100		0.999	0.287	0.975
200		1.933	0.372	0.967
300		2.681	0.602	0.990

Notes: Conditions: pH 2, m = 0.2 g.

[44,48–51,53,54]. Thus, Gibbs' free energy change of the adsorption process can be obtained using the following equation [44–54]:

$$\Delta G = -RT \ln K \quad (15)$$

where T (K) is the solution temperature, R is the gas constant (8.314 J/(mol K)), and K_d is the distribution coefficient for the adsorption. The distribution coefficient (K_d)indicates the adsorbent capability of retaining the solute and also the extent of its movement in a solution phase. It is expressed as [29,31]:

$$K_d = \frac{C_a}{C_e} \quad (16)$$

where C_a (mg) is the amount of dye uptake on the adsorbent at equilibrium. Based on van't Hoff equation, Langmuir constants (K_d) were used to determine the standard Gibbs free energy change (ΔG°), standard enthalpy change (ΔH°), and standard entropy change (ΔS°), as shown in Eqs. (17) and (18) [51]:

$$\ln K_d = -\frac{\Delta H^\circ}{RT} + \frac{\Delta S^\circ}{R} \quad (17)$$

$$\Delta G^\circ = \Delta H^\circ - T\Delta S^\circ \quad (18)$$

The values of ΔH° and ΔS° can be obtained from the slope and intercept using the plot of $\ln K_d$ vs. $1/T$. The thermodynamic parameters for the adsorption of the Alizarin Red S dye on the nano-Fe_3O_4/corn cover composite. The negative values of ΔG° (−1.51 kJ/mol at 25°C) and ΔH° (−2.81 kJ/mol) show that the adsorption processes were spontaneous and exothermic. Also, the negative values of ΔS° (−4.6 J/(mol K)) decreased the randomness during the adsorption of this dye by absorbency [54].

However the immobilization of nano-Fe_3O_4 on corn cover was found enhancing the performance adsorption capacity and increasing the life time of the biosorbents for regeneration and recycling by several orders of magnitude. Biosorbents such as agricultural waste (corn cover) containing various functional groups (carboxyl, carbonyl, hydroxyl, aromatic, and etc.) well known as efficient sorbents and stabilizes the nano-Fe_3O_4 and also prevents their oxidation and agglomeration. Therefore, integration of nano-Fe_3O_4 which has nanoparticles well-known characteristics with corn cover enhanced removal efficiency and adsorption capacity through both physi- and chemisorption process. So, combination of them would provide a low-cost and environmental-friendly adsorbent for removal of pollutants from aqueous solutions.

4. Conclusions

The efficiency of nano-Fe_3O_4/corn cover composite in removing Alizarin Red S from an aqueous solution was investigated. BBD, as a RSM, was successfully employed to obtain the optimum process conditions, while the interactions between process variables were demonstrated. The results clearly show that the dye removal efficiency was severely influenced by pH, initial concentration of dye, and also adsorbent dosage variation. The adsorption data were well fitted by the Langmuir, Freundlich, and D–R isotherms. Kinetic models, namely the pseudo-first-order, pseudo-second-order, and intraparticle diffusion for adsorption of this process were studied. The results fitted well with the pseudo-second-order kinetic model. Thermodynamic studies indicated that the adsorption process was spontaneous and exothermic in nature.

References

[1] Z. Aksu, Application of biosorption for the removal of organic pollutants: A review, Process Biochem. 40 (2005) 997–1026.
[2] G. Crini, Non-conventional low-cost adsorbents for dye removal: A review, Bioresour. Technol. 97 (2006) 1061–1085.
[3] V.G. Gupta, Suhas, Application of low-cost adsorbents for dye removal—A review, J. Environ. Manage. 90 (2009) 2013–2042.

[4] E. Forgacs, T. Cserháti, G. Oros, Removal of synthetic dyes from wastewaters: A review, Environ. Int. 30 (2004) 953–971.
[5] M. Nakayama, Sh Nakamoto, Ch Iida, M. Yoshimoto, Removal of methylene blue from aqueous solution using a polarizable nanolayered manganese oxide film, Anal. Sci. 25 (2009) 229–233.
[6] S. Pirillo, M.L. Ferreira, E.H. Rueda, The effect of pH in the adsorption of Alizarin and Eriochrome Blue Black R onto iron oxides, J. Hazard. Mater. 168 (2009) 168–178.
[7] J. Zolgharnein, N. Asanjrani, M. Bagtash, G. Azimi, Multi-response optimization using Taguchi design and principle component analysis for removing binary mixture of alizarin red and alizarin yellow from aqueous solution by nano γ-alumina, Spectrochim. Acta Part A: Mol. Biomol. Spectrosc. 126 (2014) 291–300.
[8] J. Zolgharnein, M. Bagtash, N. Asanjarani, Hybrid central composite design approach for simultaneous optimization of removal of alizarin red S and indigo carmine dyes using cetyltrimethylammonium bromide-modified TiO_2 nanoparticles, J. Environ. Chem. Eng. 2 (2014) 988–1000.
[9] A. Demirbas, Agricultural based activated carbons for the removal of dyes from aqueous solutions: A review, J. Hazard. Mater. 167(1–3) (2009) 1–9.
[10] M.R. Sohrabi, M. Ghavami, Photocatalytic degradation of Direct Red 23 dye using UV/TiO_2: Effect of operational parameters, J. Hazard. Mater. 153 (2008) 1235–1239.
[11] M. Sleiman, D.L. Vildozo, C. Ferronato, J.M. Chovelon, Photocatalytic degradation of azo dye Metanil Yellow: Optimization and kinetic modeling using a chemometric approach, Appl. Catal. B: Environ. 77 (2007) 1–11.
[12] M. Abbasi, N.R. Asl, Sonochemical degradation of Basic Blue 41 dye assisted by nanoTiO_2 and H_2O_2, J. Hazard. Mater. 153 (2008) 942–947.
[13] N. Zaghbani, A. Hafiane, M. Dhahbi, Removal of Safranin T from wastewater using micellar enhanced ultrafiltration, Desalination 222 (2008) 348–356.
[14] J.S. Wu, C.H. Liu, K.H. Chu, S.Y. Suen, Removal of cationic dye methyl violet 2B from water by cation exchange membranes, J. Membr. Sci. 309 (2008) 239–245.
[15] L. Fan, Y. Zhou, W. Yang, G. Chen, F. Yang, Electrochemical degradation of aqueous solution of Amaranth azo dye on ACF under potentiostatic model, Dyes Pigm. 76 (2008) 440–446.
[16] M.X. Zhu, L. Lee, H.H. Wang, Z. Wang, Removal of an anionic dye by adsorption/precipitation processes using alkaline white mud, J. Hazard. Mater. 149 (2007) 735–741.
[17] G. Sudarjanto, B. Keller-Lehmann, J. Keller, Optimization of integrated chemical–biological degradation of a reactive azo dye using response surface methodology, J. Hazard. Mater. 138 (2006) 160–168.
[18] V. Sarria, M. Deront, P. Peringer, C. Pulgarin, Degradation of a biorecalcitrant dye precursor present in industrial wastewaters by a new integrated iron(III) photoassisted–biological treatment, Appl. Catal. B: Environ. 40 (2003) 231–246.
[19] J. García-Montaño, L. Pérez-Estrada, I. Oller, M.I. Maldonado, F. Torrades, J. Peral, Pilot plant scale reactive dyes degradation by solar photo-Fenton and biological processes, J. Photochem. Photobiol. A: Chem. 195 (2008) 205–214.
[20] B. Lodha, S. Chaudhari, Optimization of Fenton-biological treatment scheme for the treatment of aqueous dye solutions, J. Hazard. Mater. 148 (2007) 459–466.
[21] A. Mittal, J. Mittal, L. Kurup, Batch and bulk removal of hazardous dye, indigo carmine from wastewater through adsorption, J. Hazard. Mater. 137 (2006) 591–602.
[22] B.H. Hameed, F.B.M. Daud, Adsorption studies of basic dye on activated carbon derived from agricultural waste: *Hevea brasiliensis* seed coat, Chem. Eng. J. 139 (2008) 48–55.
[23] M. Hua, S. Zhang, B. Pan, W. Zhang, L. Lv, Q. Zhang, Heavy metal removal from water/wastewater by nanosized metal oxides: A review, J. Hazard. Mater. 211–212 (2012) 317–331.
[24] M. Khajeh, S. Laurent, K. Dastafkan, Nanoadsorbents: Classification, preparation, and applications (with emphasis on aqueous media), Chem. Rev. 113(10) (2013) 7728–7768.
[25] Y.F. Shen, J. Tang, Z.H. Nie, Y.D. Wang, Y. Ren, L. Zuo, Preparation and application of magnetic Fe_3O_4 nanoparticles for wastewater, Sep. Purif. Technol. 68 (2009) 312–319.
[26] H. Heidari, H. Razmi, Multi-response optimization of magnetic solid phase extraction based on carbon coated Fe_3O_4 nanoparticles using desirability function approach for the determination of the organophosphorus pesticides in aquatic samples by HPLC–UV, Talanta 99 (2012) 13–21.
[27] J. Wang, W. Xu, L. Chen, X. Huang, J. Liu, Preparation and evaluation of magnetic nanoparticles impregnated chitosan beads for arsenic removal from water, Chem. Eng. J. 251 (2014) 25–34.
[28] J. Zolgharnein, Zh Adhami, A. Shahmoradi, S.N. Mousavi, Optimization of removal of methylene blue by platanus tree leaves using response surface methodology, Anal. Sci. 26 (2010) 111.
[29] P. Panneerselvam, N. Morad, K.A. Tan, Magnetic nanoparticle (Fe_3O_4) impregnated onto tea waste for the removal of nickel (II) from aqueous solution, J. Hazard. Mater. 186 (2011) 160–168.
[30] J. Gong, X. Wang, X. Shao, Sh. Yuan, Ch Yang, X. Hu, Adsorption of heavy metal ions by hierarchically structured magnetite-carbonaceous spheres, Talanta 101 (2012) 45–52.
[31] J. Zolgharnein, F. Gholami, N. Asanjarani, P. Zolgharnein, G. Azimi, *Platanus Carpinifolia* tree leaves as highly efficient sorbent for removal of methyl violet dye from aqueous solution; multivariate optimization, isotherm modeling, and kinetic studies, Sep. Sci. Technol. 49 (2014) 752–762.
[32] J. Zolgharnein, M. Bagtash, Hybrid central composite design optimization for removal of Methylene blue by Acer tree leaves: Characterization of adsorption, Desalin. Water Treat. 54 (2015) 2601–2610.
[33] K. Vijayaraghavan, S.W. Won, Y.-S. Yun, Single- and dual-component biosorption of reactive Black 5 and reactive Orange 16 polysulfone-immobilized esterified *Corynebacterium glutamicum*, Ind. Eng. Chem. Res. 47 (9) (2008) 3179–3185.
[34] J. Zolgharnein, M. Bagtash, T. Shariatmanesh, Simultaneous removal of binary mixture of Brilliant Green and Crystal Violet using derivative spectrophotomet-

ric determination, multivariate optimization and adsorption characterization of dyes on surfactant modified nano-γ-alumina, Spectrochim. Acta Part A: Mol. Biomol. Spectrosc. 137 (2015) 1016–1028.
[35] P. Sharma, L. Singh, N. Dilbaghi, Optimization of process variables for decolorization of Disperse Yellow 211 by *Bacillus subtilis* using Box–Behnken design, J. Hazard. Mater. 164 (2009) 1024–1029.
[36] J. Zolgharnein, A. Shahmoradi, M.R. Sangi, Optimization of Pb(II) biosorption by *Robinia* tree leaves using statistical design of experiments, Talanta 76 (2008) 528–532.
[37] J. Zolgharnein, A. Shahmoradi, J.B. Ghasemi, Comparative study of Box–Behnken, central composite, and Doehlert matrix for multivariate optimization of Pb (II) adsorption onto Robinia tree leaves, J. Chemom. 27 (2013) 12–20.
[38] M. Bezerra, R. Santelli, E. Oliveira, L.S. Villar, L.A. Escaleira, Response surface methodology (RSM) as a tool for optimization in analytical chemistry, Talanta 76 (2008) 965–977.
[39] S.L.C. Ferreira, R.E. Bruns, E.G.P. da Silva, W.N.L. dos Santos, C.M. Quintella, J.M. David, J.B. de Andrade, M.C. Breitkreitz, I.C.S.F. Jardim, B.B. Neto, Statistical designs and response surface techniques for the optimization of chromatographic systems, J. Chromatogr. A 1158 (2007) 2–14.
[40] S.L.C. Ferreira, R.E. Bruns, H.S. Ferreira, G.D. Matos, J.M. David, G.C. Brandão, E.G.P. da Silva, L.A. Portugal, P.S. dos Reis, A.S. Souza, W.N.L. dos Santos, Box-Behnken design: An alternative for the optimization of analytical methods, Anal. Chim. Acta 597 (2007) 179–186.
[41] Gh. Absalan, M. Asadi, S. Kamran, L. Sheikhian, D.M. Goltz, Removal of reactive red-120 and 4-(2-pyridylazo) resorcinol from aqueous samples by Fe_3O_4 magnetic nanoparticles using ionic liquid as modifier, J. Hazard. Mater. 192 (2011) 476–484.
[42] X.M. Guo, B. Guo, Q. Zhang, X. Sun, Absorption of 10-hydroxy camptothecin on Fe_3O_4 magnetite nanoparticles with layer-by-layer self-assembly and drug release response, Dalton Trans. 40 (2011) 3039–3046.
[43] M. Bagtash, Y. Yamini, E. Tahmasebi, J. Zolgharnein, Z. Dalirnasab, Magnetite nanoparticles coated with tannic acid as a viable sorbent for solid-phase extraction of Cd^{2+}, Co^{2+} and Cr^{3+}, Microchim. Acta 183 (2016) 449–456.
[44] Y. Liu, Y.J. Liu, Biosorption isotherms, kinetics and thermodynamics, Sep. Purif. Technol. 61 (2008) 229–242.
[45] K.Y. Foo, B.H. Hameed, Insights into the modeling of adsorption isotherm systems, Chem. Eng. J. 156 (2010) 2–10.
[46] S. Rangabhashiyam, N. Anu, M.S. Giri Nandagopal, N. Selvaraju, Relevance of isotherm models in biosorption of pollutants by agricultural byproducts, J. Environ. Chem. Eng. 2 (2014) 398–414.
[47] K.V. Kumar, K. Porkodi, F. Rocha, Isotherms and thermodynamics by linear and non-linear regression analysis for the sorption of methylene blue onto activated carbon: Comparison of various error functions, J. Hazard. Mater. 151 (2008) 794–804.
[48] H. Chen, J. Zhao, J. Wu, G. Dai, Isotherm, thermodynamic, kinetics and adsorption mechanism studies of methyl orange by surfactant modified silkworm exuviae, J. Hazard. Mater. 192 (2011) 246–254.
[49] M.-C. Shih, Kinetics of the batch adsorption of methylene blue from aqueous solutions onto rice husk: Effect of acid modified process and dye concentration, Desalin. Water Treat. 37 (2012) 200–214.
[50] J. Zolgharnein, A. Shahmoradi, P. Zolgharnein, S. Amani, Multivariate optimization and adsorption characterization of As(III) removal by using Fraxinus tree leaves, Chem. Eng. Commun. 203 (2016) 210–223.
[51] H. Tang, W. Zhou, L. Zhang, Adsorption isotherms and kinetics studies of malachite green on chitin hydrogels, J. Hazard. Mater. 209–210 (2012) 218–225.
[52] W.J. Weber Jr., J.C. Morris, Kinetics of adsorption on carbon from solution, J. Sanit. Eng. Div. ASCE 89(2) (1963) 31–59.
[53] M. Ghaedi, A. Ansari, R. Sahraei, ZnS: Cu nanoparticles loaded on activated carbon as novel adsorbent for kinetic, thermodynamic and isotherm studies of Reactive Orange 12 and Direct yellow 12 adsorption, Spectrochim. Acta Part A: Mol. Biomol. Spectrosc. 114 (2013) 687–694.
[54] A. Mittal, V. Gajbe, J. Mittal, Removal and recovery of hazardous triphenylmethane dye, Methyl Violet through adsorption over granulated waste materials, J. Hazard. Mater. 150 (2008) 364–375.